Journal of The Electrochemical Society, **149** (6) A748-A753 (2002)
0013-4651/2002/149(6)/A748/6/$7.00 © The Electrochemical Society, Inc.

The CO Poisoning Mechanism of the Hydrogen Oxidation Reaction in Proton Exchange Membrane Fuel Cells

G. A. Camara,[a] E. A. Ticianelli,[a,*,z] S. Mukerjee,[b,*] S. J. Lee,[b] and J. McBreen[b,]**

[a]*Instituto de Química de São Carlos/Universidade de São Paulo, 13560-970 São Carlos, São Paulo, Brazil*
[b]*Brookhaven National Laboratory, Energy Sciences and Technology Department, Upton, New York 11973, USA*

The CO tolerance mechanism of the hydrogen oxidation reaction was investigated on several highly dispersed carbon-supported nanocrystalline Pt and binary Pt alloys. For this purpose, current/potential behavior was derived from half-cells under actual proton exchange membrane fuel cell operating conditions and correlated with expressions derived from kinetic models. Kinetic analyses have shown that the CO poisoning effect on Pt/C, PtRu/C, and PtSn/C catalysts occurs through a free Pt site attack mechanism, involving bridge- and linear-bonded adsorbed CO. For all catalysts, the onset of CO oxidation occurs via the bridge-bonded species, but for PtRu/C and PtSn/C, the reaction starts at smaller potentials. Under this condition, the hydrogen oxidation currents are generated on the vacancies of a carbon monoxide adsorbed layer created when some of the bridge-bonded CO molecules are oxidized. The linearly adsorbed CO is oxidized at higher overpotentials, leading to an increase of the holes on the CO layer and thus of the rate of the hydrogen oxidation process.
 [DOI: 10.1149/1.1473775]

Manuscript submitted February 5, 2001; revised manuscript received January 7, 2002. Available electronically April 25, 2002.

CO tolerance is an important factor in catalyst choice for the anodic hydrogen oxidation reaction (HOR) in proton exchange membrane (PEM) fuel cells running on reformed hydrogen from methanol, natural gas, or gasoline. Gas-diffusion electrodes with a loading of 0.1-0.2 mg cm^{-2} of dispersed platinum on carbon show very small polarization losses when operating on pure H_2, but the losses are raised to unacceptable values when even small amounts of CO are present. This problem is a very active area of research. In electrocatalytic studies on smooth bulk alloy electrodes, the presence of a second element with Pt such as Ru, Sn, Os, or Mo, either alloyed or as a codeposit, yields significant improvement in the CO tolerance relative to pure Pt.[1-15] In these cases, attempts to understand the mechanism of CO poisoning have focused on a variety of experimental approaches, including the use of electrochemical techniques and *in situ* UV-visible and infrared reflectance spectroscopy.[4,7,12,16-22]

Several studies conducted at 25°C on polycrystalline smooth platinum or platinum/ruthenium surfaces have indicated that the CO poisoning mechanism occurs because of a strong adsorption of CO on the catalyst surface, which blocks the hydrogen adsorption step. Under these conditions, the hydrogen oxidation current originates only from the oxidation of M-H present on holes in the compact CO surface monolayer.[2,5] These studies indicate that both linear- and bridge-bonded adsorbed CO species can be found on the catalyst surface. This is confirmed by the fact that there is no 1:1 correspondence between the loss of an adsorbed H atom and the coverage of CO of Pt surfaces since one CO molecule can block more than one H site, as in the case of bridge-bonded CO.[4] For a platinum electrode, the linear adsorbed CO is dominant at high coverages and high electrode potentials.[16-23] Previous reports have also shown that the saturation coverage of CO at 25°C can be as high as 1 CO/Pt on polycrystalline Pt[19] and close to 0.6 CO/Pt for single-faced Pt(111), (110), and (100).[24] However, a pre-wave in the CO oxidation current-potential profile on platinum (111) and (100) single-crystal electrodes has often been ascribed to multiply bonded adsorbed CO.[24,25] The minor presence of adsorbed linear-bonded COOH[22] and CHO[26] species has also been proposed for bulk polycrystalline platinum and dispersed platinum on carbon (Pt/C) catalysts, respectively.

A previous investigation has also shown that it is possible to measure changes in the electronic (such as Pt 5d band vacancy) and short-range atomic order (such as the Pt-Pt bond distance and coordination number) with element specificity under *in situ* electrochemical conditions using X-ray absorption spectroscopy.[27,28] Application of these techniques to carbon-supported nanocrystalline PtRu and PtSn alloys has shown that the alloying changes both the electronic and the short-range atomic order.[29] For instance, alloying with Sn causes lowering of the Pt 5d band vacancies/atom and an increase in the Pt-Pt bond distance.[29] However, the effect on PtRu alloys is exactly opposite.[29] These results imply a significant change in the CO poisoning characteristics in these systems, resulting in different activation energies, reaction orders, surface coverage, etc. These in turn manifest in different electrode kinetic behavior under a variety of PEM fuel cell operating conditions.

Although these studies provided valuable information for the design of new catalysts, extrapolations of the conclusions with respect to the CO tolerance of real systems are not straightforward, mainly because of the use of reaction conditions different from the actual PEM fuel cell operating environment. Attempts to quantify the CO poisoning effect have been previously reported on phosphoric acid[30] and PEM[31-35] half-cells and single cells, simulating as closely as possible the real conditions of a fuel cell. For the PEM system, some information regarding the kinetics and mechanisms of the reactions has been obtained by using different models for the processes taking place in the electrode.[34,35] Bellows *et al.*[34] developed a CO_x inventory model for describing the behavior of adsorbed CO on Pt electrocatalysts, for hydrogen feed containing CO and CO_2. One important conclusion of this work is that, under PEM fuel cell operating conditions, CO tolerance is achieved when the rate of CO electrooxidation balances the combined adsorption fluxes from both CO and CO_2. More recently, based on a simple kinetic model involving the presence of linearly adsorbed CO, Springer *et al.*[33] have shown that, as for bulk Pt, the polarization of a Pt/C hydrogen electrode at low current densities is limited by the maximum rate of hydrogen dissociative chemisorption on a small fraction of the catalyst surface free of CO. It was also found that a rate of CO oxidation as low as 10 nA cm^{-2} (Pt) could have a significant effect in lowering the CO steady-state coverage and thus in increasing the magnitude of the hydrogen electro-oxidation current.

This paper describes the results of a kinetic analysis of the CO tolerance/poisoning effect on highly dispersed nanocrystalline Pt/C, PtRu/C, and PtSn/C catalysts. Experimental performance characteristics of half-cells under actual PEM operating conditions are correlated with expressions derived from reaction kinetics models. The treatment was developed taking into account the formation of linear- and bridge-bonded adsorbed CO and linear-bonded COOH and CHO derivatives. The CO, COOH, and CHO oxidation steps are

* Electrochemical Society Active Member.
** Electrochemical Society Fellow.
z E-mail: edsont@iqsc.sc.usp.br

also included, assuming that they may occur at different electrode potentials and depend on the nature of the catalytic material.

Experimental

Catalyst powders (20 wt % Pt, PtRu (1:1 atom %) and PtSn (3:1 atom %) supported on Vulcan XC-72 carbon) were procured from E-TEK Inc. (Natick, MA). Two series of working electrodes, prepared independently in the Brookhaven National Laboratory and Instituto de Química de São Carlos were employed. The electrodes contained a total catalyst loading of 0.4 mg cm^{-2}. The cathodes were Pt/C (20% loading, 0.4 mg cm^{-2}) gas-diffusion electrodes. The electrodes were impregnated with 1.1 mg cm^{-2} of Nafion (Aldrich Chemical Co.) and always contained 0.4 mg Pt cm^{-2}. The Nafion 115 (127 μm thick, DuPont) membrane was cleaned by treatment in boiling 3% H_2O_2, 1 M H_2SO_4, and deionized water. The membrane/electrode assemblies were prepared by hot-pressing at 130°C and 1000 kgf cm^{-2} for 2 min. The diffusional layer was made with carbon powder (Cabot) with 15% poly(tetrafluoroethylene) (Teflon TE-306A, DuPont) on a carbon cloth support (PWB-3, Stackpole).

Experiments were conducted in single cells with a geometric area of 5 cm^2 and arrangements for a reversible hydrogen reference electrode in the anode compartment, which uses the same gas stream as the working anode. The fuel cell test station was equipped with humidification chambers, mass flow controllers, back pressure regulators, and temperature controllers. Measurements were made at 85°C, with hydrogen and oxygen humidification chambers at 100 and 90°C, respectively. Reactant gas pressures were adjusted to obtain a net 0.1 MPa for the partial pressure of hydrogen and oxygen in the water vapor mixture. CO tolerance was examined in the concentration range of CO in hydrogen between 20 to 100 ppm. Both the anode and the cathode flow rates were ~250 mL/min. The polarization curves were obtained after 2 h of exposure of the anode to the corresponding reactant gas at constant cell potential (0.8 V), using a computer-controlled electronic load (HP-6050A) interfaced to an IBM/PC with Lab View software.

To avoid problems with contamination of the reference electrode, polarization of the hydrogen electrode in the presence of CO ($E_{H_2/CO}$) as a function of current density was obtained from measurements of the electrode polarization (E_{H_2}) in the absence of CO with respect to a reversible hydrogen reference electrode and the values of cell potential in the presence ($V_{H_2/CO}$) and absence of CO (V_{H_2}), by using the expression

$$E_{H_2/CO} = V_{H_2} - V_{H_2/CO} + E_{H_2}$$

The electrode overpotential was calculated at each current density using the expression

$$\eta = [E_{H_2/CO} - (E_{H_2/CO})_{J=0}]$$

Theoretical Analysis

Participation of several kinds of poisoning species was considered: the linear- and bridge-bonded adsorbed CO, and the linear-bonded CHO and COOH derivatives. In a first approach, the problem was solved assuming the presence of only linear-bonded adsorbed CO, as proposed before.[33] In other approaches, the participation of the linear-bonded CO together with one of the other adsorbates at a time was assumed. In a third approach, participation of two types of active sites for the adsorption and oxidation of both reactants (hydrogen and carbon monoxide) was assumed. These were designated as S_L and S_B and correspond to those sites promoting the adsorption of linear- and bridge-bonded CO species, respectively. The two pathways were taken as occurring in parallel and independently of each other. In this case, the theoretical treatment was developed taking into account the following possibilities for the HOR and CO adsorption and oxidation steps.

For linear adsorption sites

$$H_2(g) + 2S_L \underset{k_{-1L}}{\overset{k_{1L}}{\leftrightarrow}} 2S_LH \quad [1]$$

$$S_LH \underset{k^{\eta}_{-2L}}{\overset{k^{\eta}_{2L}}{\leftrightarrow}} S_L + H^+ + e^- \quad [2]$$

$$CO(g) + S_L \overset{k_{3L}}{\rightarrow} S_LCO \quad [3]$$

$$S_LCO + H_2O \overset{k^{\eta}_{4L}}{\rightarrow} S_L + CO_2 + 2H^+ + 2e^- \quad [4]$$

For bridge adsorption sites

$$H_2(g) + 2S_B \underset{k_{-1B}}{\overset{k_{1B}}{\leftrightarrow}} 2S_BH \quad [1a]$$

$$S_BH \underset{k^{\eta}_{-2B}}{\overset{k^{\eta}_{2B}}{\leftrightarrow}} S_B + H^+ + e^- \quad [2a]$$

$$CO(g) + 2S_B \overset{k_{3B}}{\rightarrow} (S_B)_2 = CO \quad [3a]$$

$$(S_B)_2 = CO + H_2O \overset{k^{\eta}_{4B}}{\rightarrow} 2S_B + CO_2 + 2H^+ + 2H^+ + 2e^- \quad [4a]$$

Reactions 1 and 2, or 1a and 2a correspond to the Tafel/Volmer mechanism, usually considered for the HOR in acid media.[30,35] Reactions 3 and 3a are responsible for the CO adsorption on the catalyst surface. Finally, Reactions 4 and 4a represent the CO oxidation possibilities for linear- and bridge-bonded adsorbed CO, respectively. These reactions may comprise two steps, eventually involving the formation of metal hydrous oxides, which is considered the rate-determining step.[33] To simplify the mathematical treatment and minimize the number of variables, all steps involving CO were considered totally irreversible, and the rate constants for the hydrogen adsorption/desorption (k_{1L}, k_{-1L}, k_{1B}, k_{-1B}) and oxidation (k_{2L}, k_{-2L}, k_{2B}, k_{-2B}) steps were assumed to be the same in the linear and bridge sites.

In the other approaches, in which the linear-bonded CO competes with the bridge-bonded CO for the same adsorption sites, the overall mechanism is formed by Reactions 1-4, followed by one of two possibilities

$$CO(g) + 2S_L \overset{k_5}{\rightarrow} (S_L)_2 = CO \quad [5a]$$

$$S_LCO + S_L \overset{k_5}{\rightarrow} (S_L)_2 = CO \quad [5b]$$

while for the formation of CHO and COOH adsorbates, the alternatives were

$$H_2(g) + 2S_LCO \overset{k_5}{\rightarrow} 2S_LCHO \quad [5c]$$

$$H_2(g) + S_LCO + S_L \overset{k_5}{\rightarrow} S_LCHO + S_LH \quad [5d]$$

$$S_LH + S_LCO \overset{k_5}{\rightarrow} S_LCHO + S_L \quad [5e]$$

$$S_LCO + H_2O + S_L \overset{k_5}{\rightarrow} S_LCOOH + S_LH \quad [5f]$$

In these cases, each of these reactions is followed by another step involving the oxidation of the adsorbates given by

$$(S_L)_2 = CO + H_2O \overset{k^{\eta}_6}{\rightarrow} 2S_L + CO_2 + 2H^+ + 2e^- \quad [6a]$$

$$S_LCHO + H_2O \overset{k^{\eta}_6}{\rightarrow} S_L + CO_2 + 3H^+ + 3e^- \quad [6b]$$

$$S_LCOOH + H_2O \overset{k^{\eta}_6}{\rightarrow} S_L + CO_2 + 3H^+ + 3e^- \quad [6c]$$

Since the mathematical approaches are similar in all cases, the kinetic equations and the procedure for calculations is shown only for the case in which the linear-bonded CO competes with the bridge-bonded CO for the same kind of adsorption sites (Reactions 1-4, 5a, and 6a). The time dependence of the degree of coverage of hydrogen (θ_H^L) and that of carbon monoxide (θ_{CO}^L) are given by

$$\left(\frac{d\theta_H^L}{dt}\right) = k_{1L}p_{H_2}(\theta_S^L)^2 + 2k_{-2L}^{\eta}\theta_S^L - k_{-1L}(\theta_H^L)^2 - 2k_{2L}^{\eta}\theta_H^L \quad [7]$$

$$\left(\frac{d\theta_{CO}^L}{dt}\right) = k_{3L}p_{CO}\theta_S^L - k_{4L}^{\eta}\theta_{CO}^L \quad [8]$$

$$\left(\frac{d\theta_{CO}^B}{dt}\right) = k_5 p_{CO}(\theta_S^L)^2 - k_6^{\eta}\theta_{CO}^B \quad [9]$$

where the rate constants k_{2L}^{η}, k_{-2L}^{η}, k_{4L}^{η}, and k_6^{η} are expressed in A cm^{-2}, k_{1L}, k_{-1L}, k_{3L}, and k_5 are expressed in A atm^{-1} cm^{-2}, and p_{H_2} and p_{CO} are the partial pressures of hydrogen and CO in the system expressed in atm. In these equations, the degree of coverage corresponds to values normalized for the maximum available surface sites, and thus θ_S^L is the fraction of surface sites free of any adsorbed species; that is, $\theta_S^L = 1 - \theta_H^L - \theta_{CO}^L - \theta_{CO}^B$. The current densities for the hydrogen (j_H^L) and CO (j_{CO}^L, j_{CO}^B) oxidation reactions were taken as

$$j_H^L = 2(k_{2L}^{\eta}\theta_H^L - k_{-2L}^{\eta}\theta_S^L) \quad [10a]$$

$$j_{CO}^L = 2k_{4L}^{\eta}\theta_{CO}^L \quad [10b]$$

$$j_{CO}^B = 2k_6^{\eta}\theta_{CO}^B \quad [10c]$$

The dependence of k_{2L}^{η} and k_{-2L}^{η} on the electrode overpotential (η) is expressed assuming an exponential polarization as given by the Tafel equation, that is

$$k_{2L}^{\eta} = k_{2L}\exp(\eta/b_2) \quad \text{and} \quad k_{-2L}^{\eta} = k_{-2L}\exp(-\eta/b_2) \quad [11]$$

The Tafel slope (b_2) was taken as 140 mV dec^{-1}, this value being characteristic for systems at 85°C where the Tafel/Volmer mechanism is assumed, with Volmer the rate-determining step. For CO oxidation reactions, the dependences of k_{4L}^{η} and k_6^{η} on the potential were considered to follow an exponential variation with the overpotential, eventually related to the rate of formation of surface hydrous oxides,[33] that is

$$k_{4L}^{\eta} = k_{4L}\exp(\eta/b_{4L}) \quad k_6^{\eta} = k_6\exp(\eta/b_6) \quad [12]$$

where k_{4L} and k_6 define the onset of the oxidation process, and b_{4L} and b_6 the dependence with the overpotential.[33]

Under steady-state conditions, the differential equations (Eq. 7-9) were taken as zero. Solution of this equation system to obtain θ_H^L, θ_{CO}^L, and θ_{CO}^B was made numerically after the appropriate setting of the corresponding values of rate constants and Tafel slopes. Then, the values of θ_H^L, θ_{CO}^L, and θ_{CO}^B were replaced in Eq. 10a-c, from which the current densities for the hydrogen and CO oxidation reactions were obtained as a function of the electrode overpotential.

Similar approaches were used for the kinetic treatment of all mechanistic possibilities, except for the case in which the adsorptions of linear- and bridge-bonded CO occur in parallel and independently of each other. Here, Reactions 1-4 and 1a-4a were solved separately, and the total current for the hydrogen (j_{HT}) and CO (j_{CO}) oxidations was calculated from

$$j_{HT} = (1 - f)j_H^L + fj_H^B \quad [13a]$$

$$j_{CO} = (1 - f)j_{CO}^L + fj_{CO}^B \quad [13b]$$

Table I. Values of parameters obtained by fitting the theoretical equations to the experimental results.

Kinetic parameters for the HOR
$k_{1L} = k_{1B} = 40$ A atm^{-1} cm^{-2}
$k_{-1L} = k_{-1B} = 8$ A cm^{-2}
$k_{2L} = k_{2B} = 3$ A cm^{-2}
$k_{-2L} = k_{-2B} = 2.1$ A cm^{-2}
$j_o = 1.73$ A cm^{-2}
$b_{1L} = b_{1B} = 140$ mV dec^{-1}
Kinetic parameters for the CO oxidation reaction
Pt/C: $k_{4L}/k_{3L} = 3.5 \times 10^{-8}$; $k_{4B}/k_{3B} = 2.6 \times 10^{-6}$
PtRu/C: $k_{4L}/k_{3L} = (5.2 \pm 2.5) \times 10^{-7}$; $k_{4B}/k_{3B} = (7.8 \pm 2.0) \times 10^{-7}$
PtSn/C: $k_{4L}/k_{3L} = (6.7 \pm 2.0) \times 10^{-7}$; $k_{4B}/k_{3B} = (9.5 \pm 1.5) \times 10^{-6}$
$b_{4L} = 230$ mV dec^{-1}
$b_{4B} = 1300$ mV dec^{-1}
$f = 0.1$

where f is the fraction of the total surface corresponding to bridge-bonding sites. j_{HT} was assumed to provide the total current density flowing through the electrode since it is expected to be much higher than j_{CO}.

Results and Discussion

Parameterization of the kinetic equations in absence of CO.—Because of the large number of variables, finding the appropriate set of parameters with realistic physical meaning is not straightforward. The parameterization of the kinetic equations starts with the definition of the values of the rate constants for the Tafel and Volmer reactions which are specific for the HOR and define the magnitude of the degree of coverage of adsorbed hydrogen in the absence of CO. As mentioned before, for a parallel mechanism, the theoretical lines were generated assuming the same values for the rate constants for hydrogen adsorption per square centimeter of the linear and bridge sites. Values of the kinetic parameters used in the fitting are listed in Table I, and they correspond to the same values reported by Springer *et al.*[33] The rate constants for the Tafel step were assumed to be independent of the CO coverage, which is valid for CO coverages above 0.4.[33]

According to the Tafel/Volmer mechanism, the value of k_{1L} (or k_{1B}) defines the maximum current density achieved at higher overpotentials, where the Tafel path becomes the rate-determining step. Thus, for the Pt/C catalyst under investigation, and according to the present formalism, this is 40 A cm^{-2} at 1 atm hydrogen pressure (Table I). Note that for low overpotentials, Reaction 1 or 1a can be taken as a pre-equilibrium for Reaction 2 or 2a. Thus for $\eta \rightarrow 0$, if the Langmuir isotherm is assumed for Reaction 1, it is concluded that

$$j_o \equiv k_{2L}\theta_H^L = k_{-2L}\theta_L^S \quad [14]$$

where j_o is the exchange current density for the Volmer step. In the present calculation, this value was 1.73 A cm^{-2} (Table I). Dividing by the roughness factor, the value equivalent to that of the smooth electrode at 85°C is $j_0 \cong 0.03$ A cm^{-2}. This value is in good agreement with that reported by other authors (*ca.* 0.02 A cm^{-2} at 22°C, as measured using smooth Pt in pure acid solutions[26]), particularly because it refers to a temperature of 85°C.

Polarization results in the presence of CO.—After setting the kinetic parameters for the HOR steps, fits of the theoretical equations to the experimental polarization results in the presence of CO still require appropriate evaluations of the rate constants and Tafel slopes for the CO, CHO, and COOH adsorption and oxidation steps.

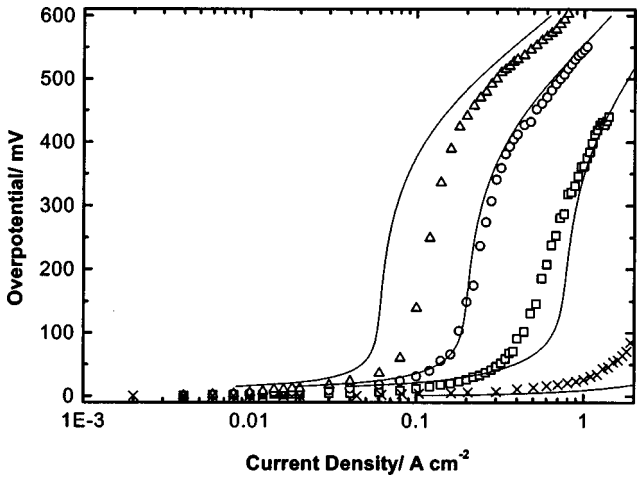

Figure 1. Fits of the experimental polarization data with the modeling equations for the HOR on Pt/C catalyst for (×) 0, (□) 20, (○) 50, and (△) 100 ppm of CO; (lines) theoretical results. Experimental results obtained at 85°C. Linear-bonded CO (Reactions 1-4). Theoretical parameters: see text.

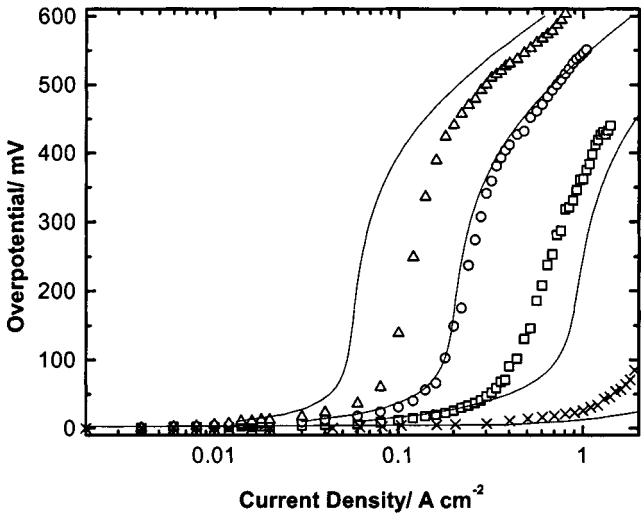

Figure 2. Fits of the experimental polarization data with the modeling equations for the HOR on Pt/C catalyst for (×) 0, (□) 20, (○) 50, and (△) 100 ppm of CO; (lines) theoretical results. Experimental results obtained at 85°C. Linear-bonded CO with participation of CHO (Reactions 1-4 plus 5d and 6b): $k_{3L}/k_{4L} = 2.4 \times 10^{-6}$; $k_5/k_6 = 2.5 \times 10^{-2}$.

The absolute values of these rate constants are not required to estimate the degree of coverages, because they always appear as a ratio, and so only the proportion between them is necessary. However, the values of the rate constants of the oxidation steps are required if the currents of CO adsorbates oxidation (Eq. 10b and c) are to be calculated.

The theoretical responses of eight different mechanistic possibilities were compared to the experimental results for the Pt/C electrode in the presence of CO. In all cases, the adjustment of the adsorption and oxidation rate constants and Tafel slopes was made using the experimental data obtained for 50 ppm of CO. Then, keeping the same group of parameters, the theoretical lines for 20 and 100 ppm CO were generated and compared to the experimental results.

Figure 1 shows the results for the mechanism involving only the linear-bonded CO (Reactions 1-4), corresponding to the same treatment presented previously.[33] Here, Reaction 3 was considered reversible and independent of CO coverage. This last assumption is reasonable since in the potential region of interest the value of θ^{L}_{CO} is essentially constant and close to 0.9. Values of rate constants and Tafel slopes resulting from the fit (Fig. 1) were $k_{3L} = 10$ A atm^{-1} cm^{-2}, $k_{-3L} = 3.5 \times 10^{-5}$ A cm^{-2}, $k_{4L} = 2.8 \times 10^{-7}$ A cm^{-2}, and $b_{4L} = 230$ mV dec^{-1}. These values of k_{3L} and k_{-3L} are in good agreement with those reported previously.[33] However, this is not the case for k_{4L} and b_{4L}, for which the published values were 1×10^{-8} A cm^{-2} and 140 mV dec^{-1}, respectively. This is not surprising since these parameters may be related to the rate of formation of Pt hydrous oxides[33] whose kinetics may be more complex than that described by Eq. 12.

Figure 2 shows the comparison of the theoretical and experimental results, considering the CHO intermediate as the second poisoning species (Reactions 1-4 plus 5d and 6b). In Fig. 1 and 2, the theoretical curves generated for 20 and 100 ppm of CO clearly do not agree with the experimental results. Similar responses were obtained for all other cases involving linear-adsorbed CHO and COOH adsorbates in combination with the linear-bonded CO. This is also the case when the bridge-bonded CO is formed by Reaction 5a or b. Figure 3 shows the fitting of the theoretical equations to the polarization data for the case in which the adsorptions of linear- and bridge-bonded CO occur in parallel and independently of each other. Here, the theoretical results generated for 20 and 100 ppm CO are in good agreement with those obtained from the experiments. The values of the kinetic parameters resulting from the fittings are presented in Table I. A value of $f = 0.1$ was assumed (Eq. 13), and this corresponds to an approximate average number, as reported previously.[4,19,22,36]

From the results in Fig. 1-3, clearly, the experimental poisoning effect of CO can only be described when the bridge-bonded species are participating in the overall reaction mechanism, but involving specific surface sites other than those promoting the linear CO adsorption. This observation is supported by results obtained for Pt single crystals[4,16,17] and also by *in situ* nuclear magnetic resonance results on Pt/C at 0.35 V.[26] This is also consistent with the fact that small platinum particles in Pt/C catalysts show a larger atomic surface fraction of Pt atoms in the (111) face than large particles.[37,38]

In Fig. 3, three regions with different characteristics are clearly seen in the curves. In the region corresponding to small overpotentials (below 20 mV), the current densities are coherent with those obtained without CO and practically independent of the CO content and of the CO-related kinetic parameters. This means that the hydrogen coverage is enough to allow Reaction 2 or 2a to occur at a fast rate. In the second range of overpotentials (from ~50 to 400

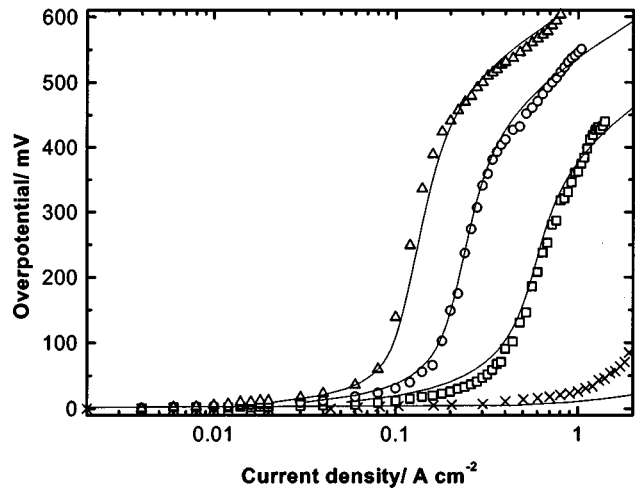

Figure 3. Fits of the experimental polarization data with the modeling equations for the HOR on Pt/C catalyst for (×) 0, (□) 20, (○) 50, and (△) 100 ppm of CO; (lines) theoretical results. Experimental results obtained at 85°C. Parallel linear- and bridge-bonded CO. Theoretical parameters in Table I.

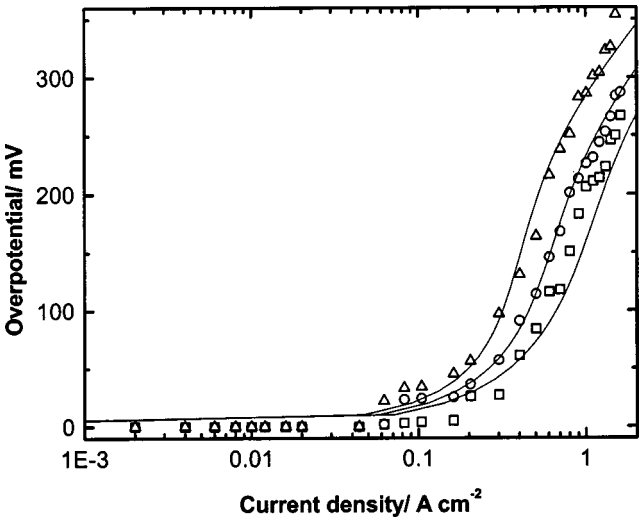

Figure 4. Fits of the experimental polarization data with the modeling equations for the HOR on PtRu/C catalyst for (□) 20, (○) 50, and (△) 100 ppm of CO. Experimental results obtained at 85°C. Theoretical parameters in Table I.

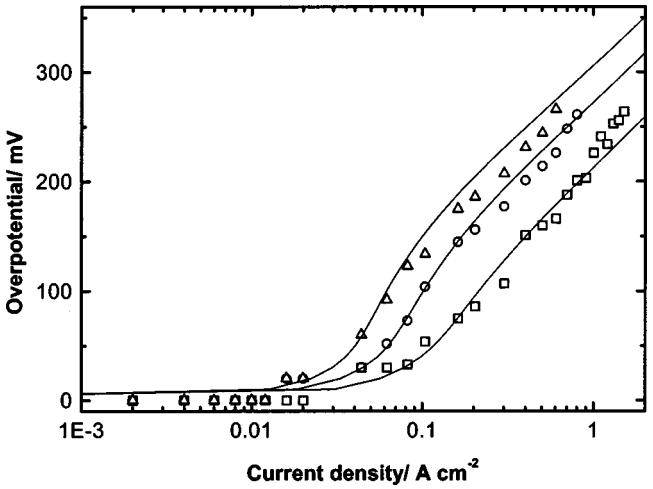

Figure 5. Fits of the experimental polarization data with the modeling equations for the HOR on PtSn/C catalyst for (□) 20, (○) 50, and (△) 100 ppm of CO. Experimental results obtained at 85°C.

mV), Reaction 1 or 1a becomes the rate-determining step, and the measured currents originate on the vacancies in the carbon monoxide adsorbed layer created when some of the CO molecules are oxidized. According to previous work,[4] these must be the multibonded CO, with a preponderant participation of bridge-bonded sites (Reaction 4a). Accordingly, in the present work, in this range, the value of the kinetic parameter k_{3B}/k_{4B} defines the magnitude of the hydrogen oxidation currents, while b_{4B} defines the dependence on the overpotential. A value of $b_{4B} = 1300$ mV dec^{-1} means that the rate of the bridge-bonded CO oxidation (Reaction 4a) has little dependence on the electrode potential and probably involves activated water molecules instead of surface hydrous oxides.[4,19]

A third region, characterized by a fast raise of the current as a function of overpotential, appears above *ca.* 0.4 V, coinciding with the beginning of a more effective CO oxidation which involves the linear bonding sites (Reaction 4). The onset overpotential of this region was closely related to the value of (k_{3L}/k_{4L}), while the dependence of the current with overpotential was closely related to the value of b_{4L}. In this new situation, the amount of holes on the CO monolayer is sufficient to permit more significant hydrogen oxidation currents.

Figures 4 and 5 present the experimental and theoretical (corresponding to the linear-bridge parallel mechanism) results for the PtRu/C and PtSn/C electrodes in the presence of CO, and Table I summarizes the values of the kinetic parameters obtained from the fits. For PtRu/C, the data in Table I correspond to the average values for two independent experiments. Also in these cases, the fittings were reasonable. The three regions of influence of the kinetic parameters on the polarization behavior are also observed. The only difference between the curves for the different catalysts is the magnitude of the currents and the onset potentials for CO oxidation steps. Also, there are no significant differences in the slope of the lines of the second and third regions for the three catalysts.

The main conclusion of this kinetic analysis is that the HOR and the CO poisoning mechanisms are the same in all catalysts, for the experimental conditions employed here. Also, the kinetic parameters for the HOR are essentially independent of the catalyst, the differences in the polarization behavior being exclusively related to the different kinetic parameters for the CO oxidation/adsorption steps.

Note in Table I that the values of k_{4L}/k_{3L} (linear sites) and k_{4B}/k_{3B} (bridge-bonded sites) are higher for PtSn/C and PtRu/C when compared to the Pt/C catalyst, indicating that the CO oxidation steps are faster in the alloys. Besides that, for all catalysts, the k_{4L}/k_{3L} values are substantially smaller than the k_{4B}/k_{3B} values, showing that the CO oxidation starts mainly at the bridge-bonded sites.

Figure 6 shows a comparison of the current density *vs.* overpotential characteristics for the HOR and the corresponding curves for the current for the CO oxidation reactions (sum of $j_{CO}{}^{L}$ and $j_{CO}{}^{B}$, Eq. 13). These last values resulted from the best fittings presented in Fig. 3-5, taking a CO concentration of 50 ppm as reference, and using $k_{3L} = k_{3B} = 10$ A atm^{-1} cm^{-2}.

In agreement with a previous observation,[33] the results presented in Fig. 6 show that, while the current densities for HOR can be of the order of 2 A cm^{-2}, the values for the current for CO oxidation are below 300 μA cm^{-2}. In Fig. 6, the onset of the CO oxidation reaction, as derived from the fits, is similar (*ca.* 0.1 V) for PtSn/C and PtRu/C, followed after some overpotential gap, by Pt/C (*ca.* 0.4 V). This behavior is consistent with the published cyclic voltammetric response,[4,39] from which a similar trend is seen for the onset of the CO oxidation reaction. The consistency between the two independent sets of results strongly supports the assumptions and valuations of physicochemical and kinetic parameters adopted in the theoretical treatment.

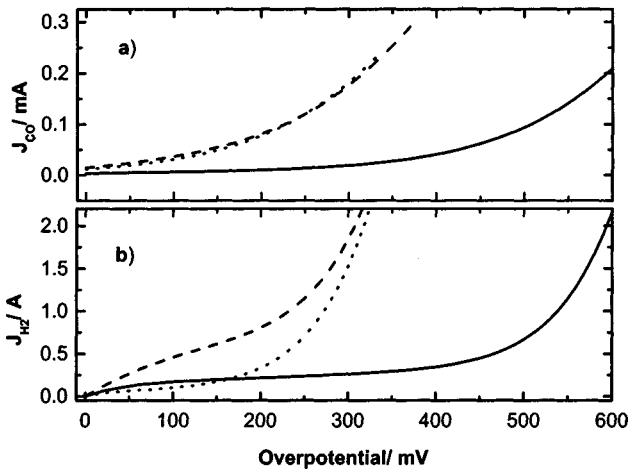

Figure 6. Simulated (a) carbon monoxide and (b) hydrogen oxidation currents for Pt/C (full line), PtRu/C (dashed line), and PtSn/C (dotted line) obtained from the same fitting as in Fig. 3-5 at $p_{CO} = 50$ ppm. Theoretical parameters in Table I.

In the simulation of the kinetics of HOR in the presence of CO, it is assumed that the hydrogen adsorption step is the same as that in the absence of the poison, that is the Tafel reaction. However, due to the high overpotential involved, some contribution to the hydrogen adsorption may also be given by the Heyrovsky reaction, as observed in neutral or alkaline solutions[40]

$$H_2 + S \leftrightarrow S - H + H^+ + e^- \qquad [15]$$

However, since the rate of this reaction increases with the reaction overpotential, it does not support the observation of a limiting current in the polarization diagram.

An important point is that, in the adsorption process on smooth electrodes, all types of hydrogen adsorption sites may be covered with CO, including sites associated with underpotential deposited hydrogen adatoms, which do not necessarily participate in the overall HOR at low overpotential.[41] As extensively discussed in the studies of the hydrogen evolution reaction on platinum[40,41] in alkaline solutions, the kinetics of the HOR in acid media at low overpotential may be governed by the coverage of more weakly bonded deposited (overpotential deposited) H atoms, in which case the CO adsorption may occur preponderantly in the bridge-bonded form. This fact would explain why at low overpotential the participation of the bridge-bonded CO is much more apparent on the analysis of the reaction kinetics.

Conclusions

Results show that the HOR and the CO poisoning mechanisms are the same in all catalysts, for the experimental conditions employed here. Also, the kinetic parameters for the HOR are essentially independent of the catalyst, the differences in the polarization behavior being exclusively related to the different reaction kinetics of the CO oxidation/adsorption steps.

In all cases, in the presence of CO the Tafel reaction becomes the rate-determining step, and the measured currents originate on the vacancies in the carbon monoxide adsorbed layer created when some of the CO molecules are oxidized. For all catalysts, the CO oxidation starts mainly at the bridge-bonded sites. Only at high overpotentials does the linearly adsorbed CO start to be oxidized, and in this new situation the amount of holes on the CO monolayer is sufficient to permit more significant hydrogen oxidation currents.

Acknowledgments

The authors thank the U.S. Department of Energy, USA, the Fundação de Amparo à Pesquisa do Estado de São Paulo (FAPESP), and the Conselho Nacional de Desenvolvimento Científico e Tecnológico (CNPq), Brazil, for their financial assistance.

Universidade de São Paulo assisted in meeting the publication costs of this article.

References

1. H. A. Gasteiger, N. Markovic, P. N. Ross, Jr., and E. J. Cairns, *J. Phys. Chem.*, **98**, 617 (1994).
2. H. A. Gasteiger, N. M. Markovic, and P. N. Ross, Jr., *J. Phys. Chem.*, **99**, 8290 (1995).
3. H. A. Gasteiger, N. M. Markovic, and P. N. Ross, Jr., *J. Phys. Chem.*, **99**, 16757 (1995).
4. K. Wang, H. A. Gasteiger, N. M. Markovic, and P. N. Ross, Jr., *Electrochim. Acta*, **41**, 2587 (1996).
5. B. N. Grgur, G. Zhuang, N. M. Markovic, and P. N. Ross, Jr., *J. Phys. Chem.*, **101**, 3910 (1997).
6. W. T. Napporn, J.-M. Léger, and C. Lamy, *J. Electroanal. Chem.*, **408**, 141 (1996).
7. K. L. Ley, R. Liu, C. Pu, Q. Fan, N. Leyarovska, C. Segree, and E. S. Smotkin, *J. Electrochem. Soc.*, **144**, 1543 (1997).
8. K. Y. Chen, P. K. Shen, and A. C. C. Tseung, *J. Electrochem. Soc.*, **142**, L185 (1995).
9. K. Y. Chen and A. C. C. Tseung, *J. Electrochem. Soc.*, **143**, 2703 (1996).
10. A. M. Castro Luna, G. A. Camara, V. A. Paganin, E. A. Ticianelli, and E. R. Gonzalez, *Electrochem. Commun.*, **2**, 222 (2000).
11. T. J. Schmidt, M. Noeske, H. A. Gasteiger, R. J. Behm, P. Britz, W. Brijoux, and H. Bönnemann, *Langmuir*, **13**, 2591 (1997).
12. W. F. Lin, T. Iwasita, and W. Vielstich, *J. Phys. Chem. B*, **103**, 3250 (1999).
13. J. Divisek, H.-F. Oetjen, V. Peinecke, V. M. Schmidt, and U. Stimming, *Electrochim. Acta*, **43**, 3811 (1998).
14. B. N. Grgur, N. M. Markovic, and P. N. Ross, *Electrochim. Acta*, **43**, 3631 (1998).
15. M. Götz and H. Wendt, *Electrochim. Acta*, **43**, 3637 (1998).
16. J. Sobkowski and A. Czerwinski, *J. Phys. Chem.*, **89**, 365 (1985).
17. B. Beden, C. Lamy, N. R. de Tacconi, and J. Arvia, *Electrochim. Acta*, **35**, 691 (1990).
18. M. Hachkar, T. Napporn, J.-M. Léger, B. Beden, and C. Lamy, *Electrochim. Acta*, **41**, 2721 (1996).
19. H. Igarashi, T. Fujino, and M. Watanabe, *J. Electroanal. Chem.*, **391**, 119 (1995).
20. Q. Fan, C. Pu, and E. S. Smotkin, *J. Electrochem. Soc.*, **143**, 3053 (1996).
21. L.-W. H. Leung, A. Wieckowski, and M. J. Weaver, *J. Phys. Chem.*, **92**, 6985 (1988).
22. Y. Zhu, H. Uchida, and M. Watanabe, *Langmuir*, **15**, 8757 (1999).
23. M. T. M. Koper, R. A. van Santen, S. A. Wasileski, and J. Weaver, *J. Chem. Phys.*, **113**, 4392 (2000).
24. Y.-T. Wong and R. Hoffmann, *J. Phys. Chem.*, **95**, 859 (1991).
25. S. Mukerjee, S. Srinivasan, M. P. Soriaga, and J. McBreen, *J. Electrochem. Soc.*, **142**, 1409 (1995).
26. B. J. Rush, J. A. Reimer, and E. J. Cairns, *J. Electrochem. Soc.*, **148**, A137 (2001).
27. S. Mukerjee and J. McBreen, in *Proceedings of the 2nd International Symposium on New Materials for Fuel Cells and Modern Battery Systems*, Montreal, pp. 548-559, July 6-10, 1997.
28. S. Mukerjee, *J. Appl. Electrochem.*, **20**, 537 (1990).
29. W. Vogel, J. Lundquist, P. Ross, and P. Stonehart, *Electrochim. Acta*, **20**, 79 (1975).
30. H. P. Dhar, L. G. Christner, A. K. Kush, and H. C. Maru, *J. Electrochem. Soc.*, **133**, 1574 (1986).
31. T. A. Zawodzinski, Jr., C. Karuppaiah, F. Uribe, and S. Gottesfeld, in *Electrode Materials and Processes for Energy Conversion and Storage IV*, J. McBreen, S. Mukerjee, and S. Srinivasan, Editors, PV 97-12 pp. 15-24, The Electrochemical Society Proceedings Series, Pennington, NJ (1997).
32. H.-F. Oetjen, V. M. Schmidt, U. Stimming, and F. Trila, *J. Electrochem. Soc.*, **143**, 3838 (1996).
33. T. Springer, T. Rockward, T. Zawodzinski, and S. Gottesfeld, *J. Electrochem. Soc.*, **148**, A11 (2001).
34. R. J. Bellows, E. P. Marucchi-Soos, and D. Terence Buckley, *Ind. Eng. Chem. Res.*, **35**, 1235 (1996).
35. K. A. Friedrich, K.-P. Geyzers, U. Linke, U. Stimming, and J. Stumper, *J. Electroanal. Chem.*, **402**, 123 (1996).
36. A. Couto, M. C. Pérez, A. Rincón, and C. Gutiérrez, *J. Phys. Chem.*, **100**, 19538 (1996).
37. G. Tamizhmani, J. P. Dodelet, and D. Guay, *J. Electrochem. Soc.*, **143**, 18 (1996).
38. K. Kinoshita, *J. Electrochem. Soc.*, **137**, 845 (1990).
39. S. J. Lee, S. Mukerjee, E. A. Ticianelli, and J. McBreen, *Electrochim. Acta*, **44**, 3283 (1999).
40. R. M. Q. Mello and E. A. Ticianelli, *Electrochim. Acta*, **42**, 1031 (1997).
41. B. E. Conway and L. Bay, *J. Electroanal. Chem.*, **198**, 149 (1986).